CMS Physics Analysis Summary

Contact: cms-pag-conveners-susy@cern.ch 2014/01/23

Search for top squarks decaying to a charm quark and a neutralino in events with a jet and missing transverse momentum

The CMS Collaboration

Abstract

A search for the pair production of light top squarks in 8 TeV pp collision events containing a jet and missing transverse momentum is presented. The data sample is collected by the CMS detector at the LHC and corresponds to an integrated luminosity of 19.7 fb^{-1}. The number of observed events is found to be consistent with the standard model contributions determined from the collision data, and limits are set down to a minimum mass difference, $m_{\tilde{t}}$ - $m_{\tilde{\chi}^0}$ of 10 GeV/c^2.

1 Introduction

Supersymmetry (SUSY) is one of the most widely studied extensions of the standard model (SM) [1–8]; proposed to potentially solve many of the problems with the SM such as a mechanism to stabilize the Higgs boson mass against radiative corrections.

In R-parity conserving SUSY, the lightest supersymmetric particle (LSP or $\widetilde{\chi}^0$) is stable and a good dark matter candidate. However, the lack of any evidence for its presence at energies probed thus far at the Large Hadron Collider (LHC) has led to looking at new ways of searching for SUSY. Compressed mass spectra, where the LSP is very close in mass to at least one of the other SUSY particles is one possibility for hidden SUSY. For example, a phenomenologically well motivated scenario puts the mass difference between the lighter top squark ($\widetilde{\mathrm{t}}$) and the LSP as 80 GeV/c^2 or less, resulting in $\widetilde{\mathrm{t}} \to c\widetilde{\chi}^0$ decays [9–12]. In such scenarios, the charm jet is expected to be relatively soft and hidden by low energy QCD background events or too soft for the CMS detector to identify.

SUSY searches typically require events with energetic multijet final states, missing transverse energy and/or leptons. Soft visible final states arising from these compressed spectra scenarios would be indistinguishable from the QCD backgrounds in such searches. Rather than focusing triggering and event selections on discriminating soft charm jets from SM backgrounds, looking for particles produced in association with such decays offers scope for searching for compressed spectra. These interactions can be detected if they are accompanied by initial state radiation (ISR), produced in a boosted system. Provided final state particles are invisible, such events contain a high p_{T} jet and missing energy; a monojet signal thus arises.

In this analysis, we present a search for top squarks in events with one or two jets and a large imbalance in transverse momentum in pp collisions at a center-of-mass energy $\sqrt{s} = 8$ TeV corresponding to an integrated luminosity of 19.7 fb^{-1}. These data were collected using the CMS detector at the LHC. For a small mass difference, the top squark can not decay into a W boson, b-quark and an LSP, and decays primarily into a charm quark and an LSP through loop-induced two body decays [13]. In this search, the top squark is assumed to always decay to $c\widetilde{\chi}^0$ and the branching fractions to the three-body decay $\widetilde{\mathrm{t}} \to b\mathrm{W}\widetilde{\chi}^0$ and four-body decay $\widetilde{\mathrm{t}} \to bf\bar{f}\widetilde{\chi}^0$ [14] are assumed to be negligible. Squarks and gluinos are assumed to be decoupled from the third generation squarks. This analysis closely follows the procedure described in [15].

2 The CMS detector and event reconstruction

CMS uses a right-handed coordinate system in which the z axis points in the anticlockwise beam direction, the x axis points towards the center of the LHC ring, and the y axis points up, perpendicular to the plane of the LHC ring. The azimuthal angle ϕ is measured in the x-y plane, and the polar angle θ is measured with respect to the z axis. A particle with energy E and momentum $\vec{p}$ is characterized by transverse momentum $p_{\mathrm{T}} = |\vec{p}| \sin\theta$, and pseudorapidity $\eta = -\ln[\tan(\theta/2)]$.

The CMS superconducting solenoid, 12.5 m long with an internal diameter of 6 m, provides a uniform magnetic field of 3.8 T. The inner tracking system is composed of a pixel detector with three barrel layers at radii between 4.4 and 10.2 cm and a silicon strip tracker with 10 barrel detection layers extending outwards to a radius of 1.1 m. This system is complemented by two endcaps, extending the acceptance up to $|\eta| = 2.5$. The momentum resolution for reconstructed tracks in the central region is about 1% at $p_{\mathrm{T}} = 100$ GeV/c. The calorimeters inside

the magnet coil consist of a lead tungstate crystal electromagnetic calorimeter (ECAL) and a brass-scintillator hadron calorimeter (HCAL) with coverage up to $|\eta| = 3$. The quartz/steel forward hadron calorimeters extend the calorimetry coverage up to $|\eta| = 5$. The HCAL has an energy resolution of about 10% at 100 GeV for charged pions. Muons are measured up to $|\eta| < 2.4$ in gas-ionization detectors embedded in the flux-return yoke of the magnet. A full description of the CMS detector can be found in Ref. [16].

Particles in an event are individually identified using particle-flow reconstruction [17]. This algorithm reconstructs each particle produced in a collision by using an optimised combination of information from the tracker, the calorimeters, and the muon system, and identifies them as either charged hadrons, neutral hadrons, photons, muons, or electrons. These particles are used as inputs to the anti-k_T jet clustering algorithm [18] with a distance parameter of 0.5. Jet energies are corrected to particle level with p_T- and η-dependent correction factors. These corrections are derived from Monte Carlo (MC) simulation and, for data events, are supplemented by a correction derived by measuring the p_T balance in dijet events from collision data [19]. The missing transverse momentum (E_T^{miss}) in this analysis is defined as the magnitude of the vector sum of the transverse momentum of all particles reconstructed in the event, excluding muons. This definition allows the use of a control sample of $Z \to \mu\mu$ events for estimating the $Z \to \nu\nu$ background.

Muons are reconstructed by finding compatible track segments in the silicon tracker and the muon detectors [20] and are required to be within $|\eta| < 2.4$. Electron candidates are reconstructed starting from a cluster of energy deposits in the ECAL that is then matched to the momentum associated with a track in the silicon tracker. Electron candidates are required to have $|\eta| < 1.44$ or $1.56 < |\eta| < 2.5$ to avoid poorly instrumented regions. Muon and electron candidates are required to originate within 2 mm of the beam axis in the transverse plane. A relative isolation parameter is defined as the sum of the p_T of the charged hadrons, neutral hadrons, and photon contributions computed in a cone of radius 0.3 around the lepton direction, divided by the lepton p_T. Lepton candidates with relative isolation values below 0.2 are considered isolated.

Hadronically decaying taus are reconstructed using the "hadron-plus-strips" (HPS) algorithm [21], which reconstructs candidates with one or three charged pions and up to two neutral pions.

3 Monte Carlo event generation

The signal samples have been generated using the leading order (LO) matrix element event generator MADGRAPH 5 [22] with up to 2 partons and interfaced with PYTHIA 6.42 [23] with tune Z2star [24] for parton showering and hadronization and the CTEQ 6L1 [25] parton distribution functions (PDF). The samples consist of 42 mass points covering the range of phase space ($m_{\tilde{t}}, m_{\tilde{t}} - m_{\tilde{\chi}^0}$) = ($100 \leq m_{\tilde{t}} \leq 250\,\text{GeV}/c^2$, $10 \leq m_{\tilde{t}} - m_{\tilde{\chi}^0} \leq 80\,\text{GeV}/c^2$). The signal samples are Simplified Model Spectra (SMS) [26]. The use of the simplified model framework allows one to quantify the dependence of the experimental limit of a $\tilde{t} \to c\tilde{\chi}^0$ with 100% branching fraction in a manner that is more general than the constrained minimal supersymmetric Standard Model.

The parton showering program generates partons in a phase space that overlaps with the phase space of the partons generated by the matrix element calculator. Double-counting by the matrix element calculation and parton showering is resolved by using the MLM matching prescription [27], as implemented in [22]. Samples have been generated with the CMSSW FastSim program, which has been fully validated and tuned with the full GEANT-based CMS simula-

tion.

The Z+jets, W+jets, $t\bar{t}$, and single-top event samples are produced using MADGRAPH interfaced with PYTHIA 6.42, using tune Z2star and the CTEQ 6L1 PDFs. The Z+jets and W+jets samples are generated with a cut on the transverse momentum of the boson, $p_T > 100$ GeV/c. The QCD multijet sample is generated with PYTHIA 6.42, using tune Z2star and CTEQ 6L1 PDFs. The diboson WW, WZ, ZZ and W+gamma samples are generated with PYTHIA 6.42, using tune Z2star and CTEQ 6L1 PDFs. The Z+gamma samples are produced using MADGRAPH interfaced with PYTHIA. In order to avoid double counting photons from the PYTHIA shower in W+jets and W+gamma samples (and similarly for Z+jets), we remove events from the W+jets simulation which have a photon from ISR or final state radiation (FSR), of $p_T(\gamma) > 5$ GeV/c. All the generated background events are passed through a GEANT4 [28] simulation of the CMS detector.

4 Event selection

The data used in this analysis are recorded by two triggers, one that requires $E_T^{miss} > 120$ GeV as measured online by the trigger system, where the E_T^{miss} is calculated using the calorimeter information only. The second trigger requires a particle-flow jet with $p_T > 80$ GeV/c within $|\eta| < 2.6$ and for less than 95% of the jet energy in the electromagnetic calorimeter to be carried by neutral hadrons. In addition, it requires $E_T^{miss} > 105$ GeV, where the E_T^{miss} is reconstructed using the particle-flow algorithm and excludes muons. Events are required to have at least one well-reconstructed primary vertex [29]. To suppress the instrumental and beam-related backgrounds, events are rejected if less than 20% of the energy of the highest p_T jet is carried by charged hadrons or more than 70% of this energy is carried by either neutral hadrons or photons.

Such spurious jets primarily arise from instrumental noise, where the energy deposition is limited to one sub-detector. Jets resulting from energy deposition by beam halo or cosmic-ray muons do not have associated tracks and are also rejected by these selections. The application of these data cleanup requirements are very effective in rejecting non-collision backgrounds.

Events are required to have $E_T^{miss} > 250$ GeV and the jet with the highest transverse momentum (j_1) is required to have $p_T(j_1) > 110$ GeV/c and $|\eta(j_1)| < 2.4$. The triggers used to collect these data are fully efficient for events passing these selection cuts. To increase signal acceptance, a second jet (j_2) is allowed. As signal events contain both a jet from ISR or FSR and (soft) charm jets, the second jet is required to have $p_T > 60$ GeV/c, $|\eta| < 4.5$. The p_T requirement on the second jet keeps soft charm jets 'invisible' while maintaining a low QCD contribution; as the jet counting threshold is raised further more QCD multijet events fall below threshold and the QCD background increases. Jets must pass a loose PF jet ID, which helps to remove events where a photon fakes a jet, and $\Delta\phi(j_1, j_2) < 2.5$. The angular requirement between the two jets suppresses QCD dijet events. Events with more than two jets with p_T above 60 GeV/c and $|\eta| < 4.5$ are discarded.

To reduce background from Z and W production and top-quark decays, events with well reconstructed and isolated electrons with $p_T > 10$ GeV/c and $|\eta| < 2.5$, and muons reconstructed with $p_T > 10$ GeV/c and $|\eta| < 2.4$ are rejected. Events with a well identified tau with $p_T > 20$ GeV/c and $|\eta| < 2.3$ are also removed. The analysis is performed in 7 inclusive regions of leading jet p_T: $p_T(j_1) > 250$, 300, 350, 400, 450, 500, and 550 GeV/c.

The $p_T(j_1)$, $\eta(j_1)$, N_{jets}, and $\Delta\phi(j_1, j_2)$ distributions are shown in Fig. 1. The E_T^{miss} distribution

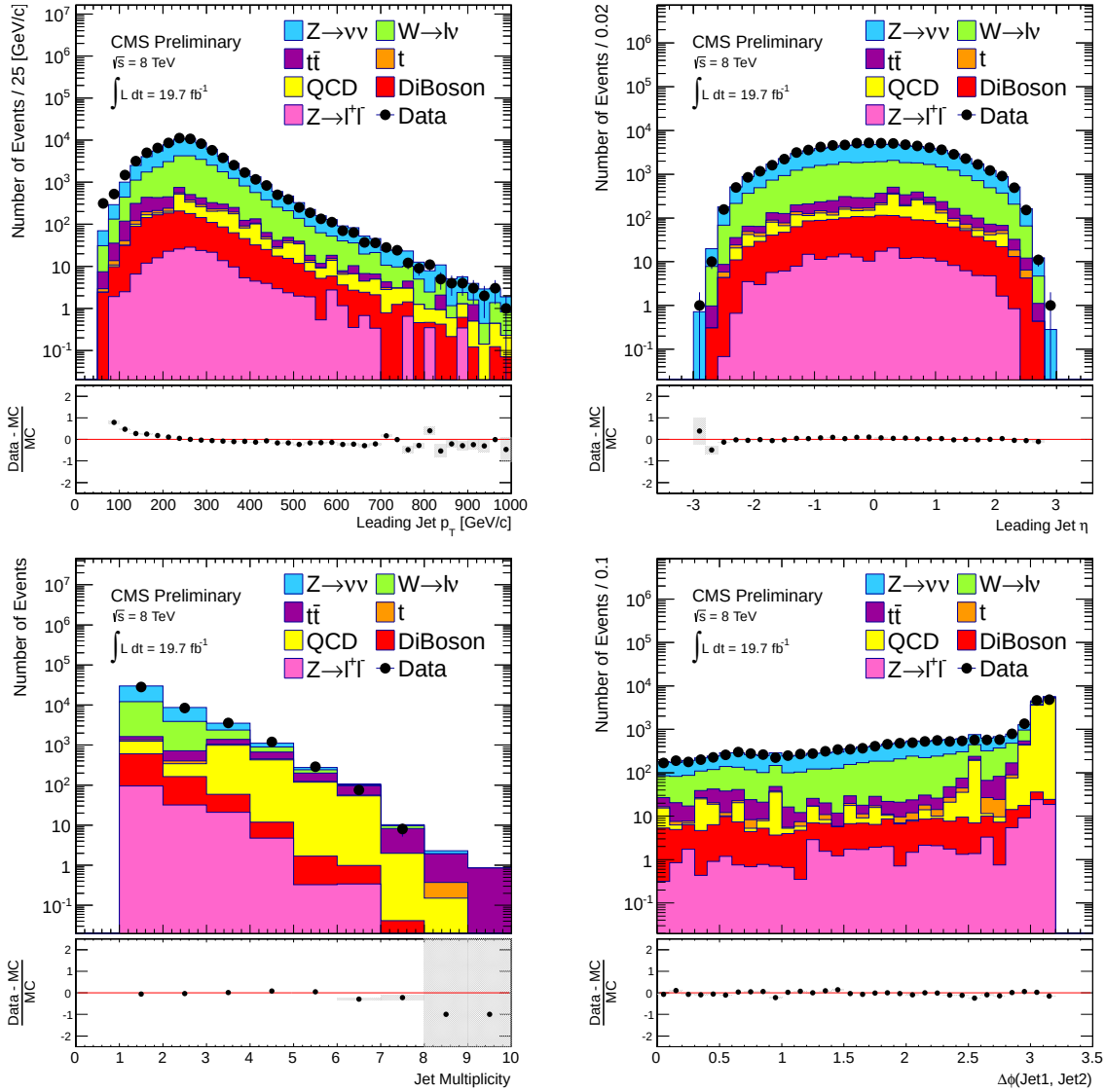

Figure 1: Plots of basic selection variables for jets with all cuts applied except on the variable plotted. Discrepancy between data and simulation in the first few bins of $p_{\mathrm{T}}(\mathrm{j}_1)$ is due to mis-modelling of ISR. These bins are cut out into inclusive signal regions, where the minimum $p_{\mathrm{T}}(\mathrm{j}_1)$ is 250 GeV/c. For the jet multiplicity and the $\Delta\phi(j_1, j_2)$ distributions, the leading jet is required to have $p_{\mathrm{T}} > 110$ GeV/c and $|\eta| < 2.4$, and the second jet is required to have $p_{\mathrm{T}} > 60$ GeV/c and $|\eta| < 4.5$. The leading SM backgrounds from $\mathrm{Z} \to \nu\nu$ and W+jet events are normalised using a data-driven technique.

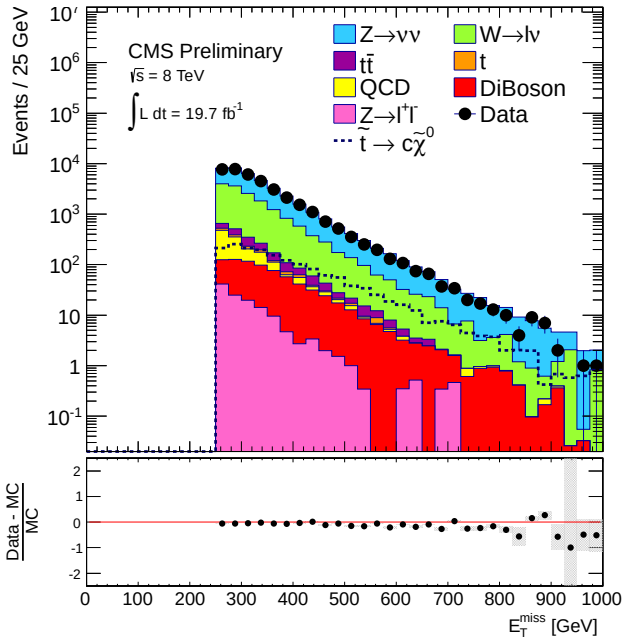

Figure 2: Missing transverse momentum $E_{\mathrm{T}}^{\mathrm{miss}}$ after all selection cuts for data and SM backgrounds. A representative signal distribution for $\tilde{t} \to c\tilde{\chi}^0$ is also shown, where $m_{\tilde{t}} = 250\,\mathrm{GeV}/c^2$, $m_{\tilde{\chi}^0} = 240\,\mathrm{GeV}/c^2$.

from data and the expected backgrounds after all selection criteria and requiring $p_{\mathrm{T}}(\mathrm{j}_1) > 110$ GeV/c is shown in Fig. 2.

Table 1 lists the number of background events obtained from the simulation at each step of the analysis event selection, where 'Preselection' includes jet cleaning requirements and the following cuts for which the trigger is fully efficient; $E_{\mathrm{T}}^{\mathrm{miss}} > 200$ GeV, $p_{\mathrm{T}}(\mathrm{j}_1) > 110\,\mathrm{GeV}/c$ and $|\eta(\mathrm{j}_1)| < 2.4$. A further cut of $E_{\mathrm{T}}^{\mathrm{miss}} > 250$ GeV is made concurrently with the initial $p_{\mathrm{T}}(\mathrm{j}_1) > 250\,\mathrm{GeV}/c$ selection. Here, W+jets and $\mathrm{Z} \to \nu\nu$+jets are normalised to the LO cross sections; these are later estimated with data driven methods. Z+jets events are normalised to the NNLO cross section and diboson events (WW, WZ and ZZ) are normalised to NLO cross sections. To ensure QCD simulation agrees reasonably well with data, the QCD rich control region $\Delta\phi(E_{\mathrm{T}}^{\mathrm{miss}}, \mathrm{j}_2) < 0.3$ is used to normalise QCD events. $\mathrm{t\bar{t}}$ events are normalised to the NNLO cross section. More information on these normalisations can be found in Section 5. The dominant background in the signal region is $\mathrm{Z} \to \nu\nu$+jets, followed by W+jets.

5 Background estimate from data

Table 1 shows that the SM backgrounds remaining after the full event selection are dominated by the following processes: Z+jets with the Z boson decaying into a pair of neutrinos and W+jets with the W boson decaying leptonically. These backgrounds are estimated from data utilizing a control sample of μ+jet events, which is derived from the same dataset as used for the signal search (using the same triggers). The monojet event selection is applied, with the exception of the lepton vetoes. From this lepton rich data sample, $\mathrm{Z} \to \mu\mu$ events are used to estimate the $\mathrm{Z} \to \nu\nu$ background and $\mathrm{W} \to \mu\nu$ events are used to estimate the remaining W+jets background.

The sample of $\mathrm{Z} \to \mu\mu$ events is selected by requiring two muons with $p_{\mathrm{T}} > 20$ GeV/c and

Table 1: Number of events selected at each step of the analysis and for the $p_T(j_1)$ regions. Backgrounds are obtained from MC and normalised as described in the text. Also shown are the cross sections used for each process.

Selection	W+jets	Z+jets	$Z \to \nu\nu$+jets	$t\bar{t}$	QCD	Single top	Diboson	Total MC
Cross section (pb)	228.9	40.5	588.3	234.0	1.1e6	114.8	105.7	
Trigger	2514352	190332	4337526	65666	461413	77284	5429269	13075841
$E_T^{miss} > 200$ GeV	317656	30242	134578	9572	63174	9289	87605	652117
Noise Cleaning	292550	27880	123420	8706	59412	8525	81668	602162
$p_T(j_1) > 110$ GeV/c	279323	26652	117513	8045	53353	7752	80844	573484
$N_{Jets} \leq 2$	254058	24413	109313	7287	29364	5596	44247	474278
$\Delta\phi(j_1, j_2) < 2.5$	237533	22947	104158	6984	25312	4815	8433	410181
Muon veto	106236	1511	104152	4051	9826	1892	7444	235112
Electron veto	79407	1004	104065	3459	6557	1325	7401	203218
Tau veto	71808	807	103106	3248	5599	1147	7047	192762
$p_T(j_1) > 250$ GeV/c, $E_T^{miss} > 250$ GeV	13641	127	22615	639	602	172	819	38615
$p_T(j_1) > 300$ GeV/c	6873	75	11093	369	344	97	546	19397
$p_T(j_1) > 350$ GeV/c	3182	40	5231	206	178	49	332	9218
$p_T(j_1) > 400$ GeV/c	1501	25	2617	113	91	21	181	4549
$p_T(j_1) > 450$ GeV/c	751	17	1335	64	48	11	92	2318
$p_T(j_1) > 500$ GeV/c	376	11	727	36	27	5.2	61	1244
$p_T(j_1) > 550$ GeV/c	204	7.4	406	21	18	3.2	34	693

$|\eta| < 2.1$, with at least one muon also passing the isolation cut. The requirements on muons for this control sample are tighter than used in the lepton veto, to ensure a clean, well identified set of muons. The dimuon reconstructed invariant mass is required to be between 60 and 120 GeV/c^2. Table 2 shows the event yields obtained for the $Z \to \mu\mu$ control sample and the predicted backgrounds from MC.

Table 2: Event yields for the $Z \to \mu\mu$ data control sample and the backgrounds from MC. Total uncertainty on the MC yield is $< 50\%$; each contribution is assigned 50% error and uncertainties are combined in quadrature.

	Z+jets	W+jets	$Z \to \nu\nu$	$t\bar{t}$	Single t	QCD	Diboson	All MC	Data
$p_T(j_1) > 250$ GeV/c	3067	0	0	37	5.7	0	68	3177	2547
$p_T(j_1) > 300$ GeV/c	1577	0	0	21	2.2	0	41	1641	1235
$p_T(j_1) > 350$ GeV/c	757	0	0	9.9	0.9	0	24	791	567
$p_T(j_1) > 400$ GeV/c	382	0	0	4.8	0.9	0	13	401	277
$p_T(j_1) > 450$ GeV/c	198	0	0	0.7	0	0	8.2	207	150
$p_T(j_1) > 500$ GeV/c	109	0	0	0	0	0	4.4	113	79
$p_T(j_1) > 550$ GeV/c	62	0	0	0	0	0	2.6	65	40

The dimuon invariant mass and dimuon p_T distributions in the data control sample and the simulation for a E_T^{miss} cut of 250 GeV are shown in Fig. 3.

The production of a Z boson in association with jets and its subsequent decay into neutrinos has similar kinematic characteristics to Z+jets events where the Z boson decays to muons. By treating the pair of muons as a pair of neutrinos, the topology of the $Z \to \nu\nu$ process is reproduced. The number of $Z \to \nu\nu$ events can then be predicted using:

$$N(Z \to \nu\nu) = \frac{N^{obs} - N^{bgd}}{A \times \epsilon} \cdot R \quad (1)$$

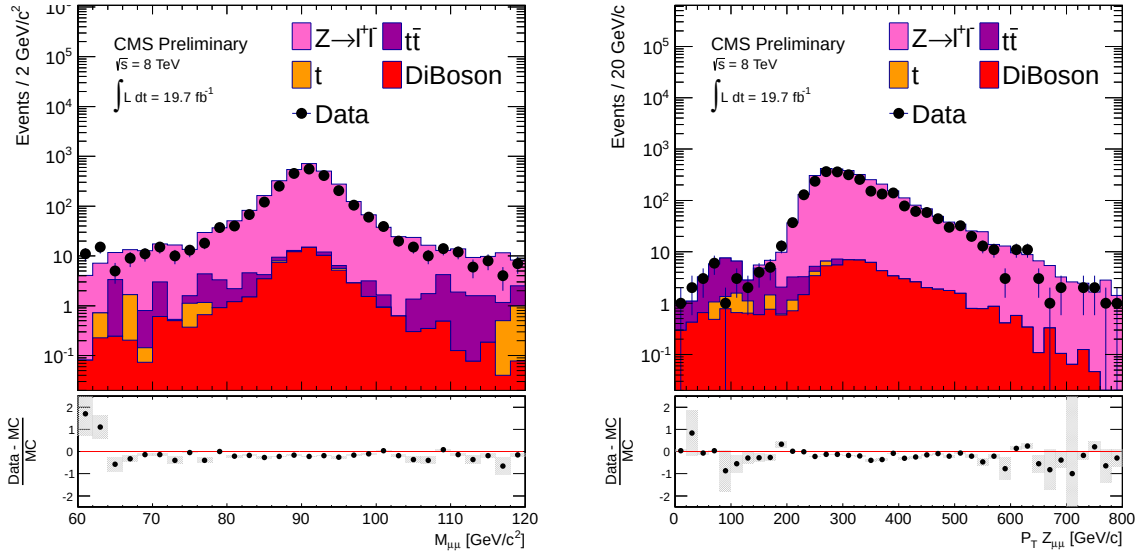

Figure 3: The dimuon invariant mass and dimuon p_{T} distributions for data (black full points with error bars) and simulation (histogram) for $60 < M_{\mu\mu} < 120\,\mathrm{GeV}/c^2$. There is no significant non-Z background.

Table 3: Data-driven prediction of $Z \to \nu\nu$+jets events for different $p_{\mathrm{T}}(j_1)$ regions.

$p_{\mathrm{T}}(\mathrm{j_1})$	> 250	> 300	> 350	> 400	> 450	> 500	> 550
$Z \to \nu\nu$	21209±1115	10077±592	4597±324	2250±197	1250±137	663±94	334±65

where N^{obs} is the number of dimuon events observed, N^{bgd} is the estimated number of background events contributing to the dimuon sample, A is the acceptance, and ϵ is the selection efficiency for the event. The acceptance A is defined as the fraction of simulated events that pass all signal selection requirements (except muon veto) and have two muons with $p_{\mathrm{T}} > 20\,\mathrm{GeV}/c$ and $|\eta| < 2.1$ and with an invariant mass within the Z mass window, calculated using Z+jets simulation. The selection efficiency ϵ is defined as the fraction of events that have two reconstructed muons passing identification and isolation cuts, with $p_{\mathrm{T}} > 20\,\mathrm{GeV}/c$ and $|\eta| < 2.1$ and with an invariant mass within the Z mass window of 60 to 120 GeV/c, given they are within the acceptance. The muon selection efficiency is also estimated from Z+jets simulation but corrected to account for differences in the measured muon efficiency between data and MC. R is the ratio of branching fractions for the Z decay to a pair of neutrinos and to a pair of muons, $R = BF(Z \to \nu\nu)/BF(Z \to \mu\mu) = 5.942 \pm 0.019$ [30]. R is corrected for contamination from virtual photon exchange in the Z+jets sample and for the Z mass window restricting phase space, and 2% uncertainty is assigned to it.

The final prediction for the number of $Z \to \nu\nu$+jets events is given in Table 3. The uncertainty on the prediction includes both statistical and systematic contributions. The sources of uncertainty are: (i) the statistical uncertainty on the number of $Z \to \mu\mu$ events in the data and simulation, (ii) a 50% uncertainty from backgrounds taken from MC, (iii) uncertainties associated with parton distribution function choice (2%) [31–33] as recommended in [34], (iv) the uncertainty in the selection efficiency ϵ as determined from the e in measured efficiencies in data and MC simulation, including a 2% uncertainty due to hadronization and (v) a 2% uncertainty on R. A summary of the contributions of these uncertainties, added in quadrature (where A and

Table 4: Summary of the contributions (in %) to the total uncertainty on the $Z \to \nu\nu$ background from the various factors used in the data-driven estimation.

$p_T(j_1)$	> 250	> 300	> 350	> 400	> 450	> 500	> 550
Statistics (N^{obs})	2.1	3.0	4.5	6.5	8.7	12	17
Background (N^{bgd})	1.6	2.0	2.4	2.7	2.9	2.9	3.5
Acceptance	2.0	2.1	2.1	2.2	2.4	2.5	2.9
Efficiency	2.1	2.1	2.3	2.6	3.3	4.4	5.5
R	2.0	2.0	2.0	2.0	2.0	2.0	2.0
Total	5.3	5.9	7.0	8.8	11	14	19

ϵ are considered to be correlated) to get the total error on the $Z \to \nu\nu$ background, is shown in Table 4.

The second largest background arises from W+jets events that are not removed by the lepton veto. These events can come from W decays in which the lepton (electron or muon, including leptonically decaying taus) is either not identified, not isolated, or out of the acceptance region, or events in which a tau decays hadronically. Contributions to the signal sample from these events where the lepton is 'lost' are estimated from the $W \to \mu\nu$+jets control sample, derived from the same set of triggers as those used for signal search.

A $W \to \mu\nu$ sample is selected by requiring an isolated muon with $p_T > 20\,\text{GeV}/c$ and $|\eta| < 2.1$ and the transverse mass M_T to be between 50 and $100\,\text{GeV}/c^2$. The transverse mass is defined as $M_T = \sqrt{2p_T^\mu E_T^{\text{miss}}\,(1-\cos(\Delta\phi))}$, where p_T^μ is the transverse momentum of the muon and $\Delta\phi$ is the angle between the muon p_T and the E_T^{miss} vectors. Table 5 shows the event yields obtained from the $W \to \mu\nu$ control sample and the predicted backgrounds from MC. Figure 4 shows the W transverse mass and transverse momentum distributions for data and simulation in the $W \to \mu\nu$ control sample.

Table 5: Event yields for the $W \to \mu\nu$ data control sample and the backgrounds from MC. Total uncertainty on the MC yield is $< 50\%$; each contribution is assigned 50% error and uncertainties are combined in quadrature.

	W+jets	Z+jets	$Z \to \nu\nu$	$t\bar{t}$	Single t	QCD	Diboson	All MC	Data
$p_T(j_1)$ >250 GeV/c	11436	183	0	608	158	0.3	197	12582	11371
$p_T(j_1)$ >300 GeV/c	5712	94	0	313	80	0.3	121	6320	5477
$p_T(j_1)$ >350 GeV/c	2694	44	0	151	41	0.3	71	3001	2547
$p_T(j_1)$ >400 GeV/c	1349	22	0	76	22	0.3	41	1509	1258
$p_T(j_1)$ >450 GeV/c	712	9.9	0	41	13	0.3	22	798	668
$p_T(j_1)$ >500 GeV/c	389	6.6	0	20	7.8	0.3	13	437	352
$p_T(j_1)$ >550 GeV/c	223	3.7	0	11	4.8	0.3	6.5	249	184

$W \to \mu\nu$ candidate events (N^{obs}), after subtracting non-W contamination (N^{bgd}), (taken from the non W+jets events in Table 5) are corrected for the detector acceptance (A') and selection efficiency (ϵ') to obtain the total number of produced events $N_{\text{tot}\,\mu} = (N^{\text{obs}} - N^{\text{bgd}})/(A' \times \epsilon')$. This number is subsequently weighted by the inefficiency of the selection criteria used in the muon veto to predict the number of events that are not rejected by the veto and thus remain in the signal sample.

The total background from $W \to \mu\nu$+jet events that are 'lost' because they are either out of the

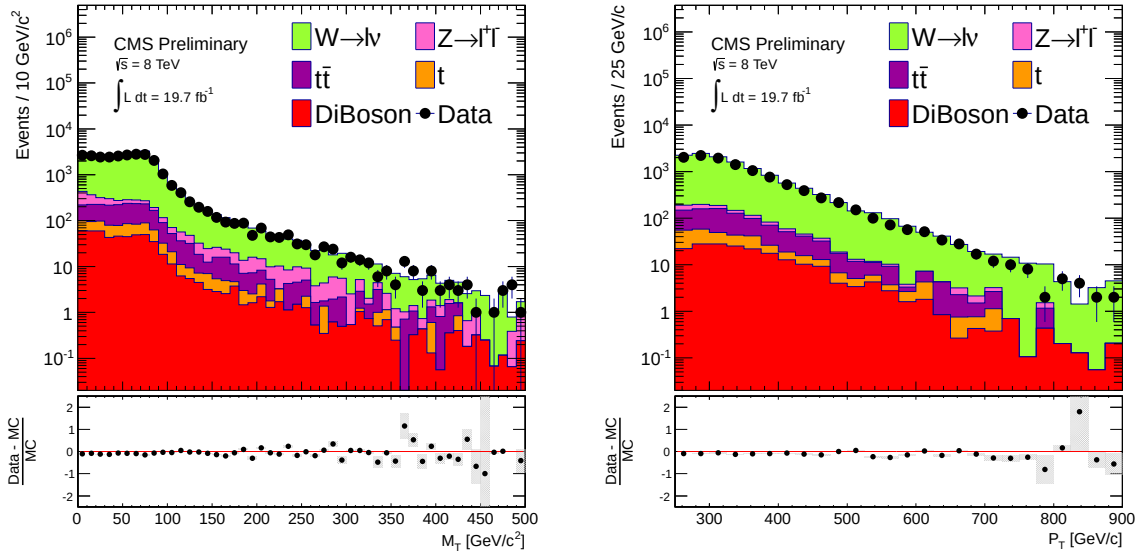

Figure 4: Distributions of the transverse mass M_{T} (left) of the muon and the transverse momentum of the muon in the W mass window, 50 - 100 GeV/c^2, (right) in the W $\rightarrow \mu\nu$ control sample, compared with MC predictions for W $\rightarrow \mu\nu$, $\mathrm{t\bar{t}}$, Z $\rightarrow \mu\mu$ and single-top production.

Table 6: Data-driven prediction of W+jets events for different $p_{\mathrm{T}}(j_1)$ regions.

$p_{\mathrm{T}}(\mathrm{j_1})$ (GeV/c)	> 250	> 300	> 350	> 400	> 450	> 500	> 550
W+jets	12328±707	5939±366	2690±180	1246±92	627±52	301±29	150±18

acceptance or are not identified or are not isolated can be written as:

$$N_{\mathrm{lost}\,\mu} \quad = \quad N_{\mathrm{tot}\,\mu} \times (1 - A_\mu \epsilon_\mu) \tag{2}$$

where A_μ is the acceptance, and ϵ_μ is the efficiency of the muon selection used in the lepton veto.

An estimate of the 'lost' electron background is obtained in a similar way from the W $\rightarrow \mu\nu$+jets data sample, using $N_{\mathrm{tot}\,\mu}$. To get the total number of produced electron events, the ratio of the produced W $\rightarrow \mu\nu$ and W $\rightarrow$ eν events passing the signal selection is taken from W+jets simulation and used to obtain $N_{\mathrm{tot}\,e}$. The same procedure is then applied to obtain the number of events where the electron is either not reconstructed or not isolated or out of the acceptance to get the total background from 'lost' electrons from W $\rightarrow$ eν events.

The remaining component of the W+jets background from events where the W decays to a tau lepton and the tau decays hadronically is estimated using the same method. The ratio of the produced W $\rightarrow \mu\nu$ and W $\rightarrow \tau\nu$ events are used to obtain the total number of produced tau events, $N_{\mathrm{tot}\,\tau}$. This is subsequently multiplied by the inefficiency of the tau selection used in the veto to obtain the remaining W background from 'lost' taus.

The detector acceptance for electrons, muons and taus is obtained from simulation. The selection efficiency is also obtained from simulation but corrected for any difference in the efficiency measured in data and simulation.

The final prediction for the number of W+jets from the sum of $N_{\mathrm{lost}\,\mu}$, $N_{\mathrm{lost}\,e}$, $N_{\mathrm{lost}\,\tau}$ events is given in Table 6. The uncertainty on the prediction includes both statistical and system-

Table 7: Summary of the contributions (in %) to the total uncertainty on the W+jets background from the various factors used in the data-driven estimation.

$p_{\mathrm{T}}(\mathrm{j}_1)$ (GeV/c)	> 250	> 300	> 350	> 400	> 450	> 500	> 550
Statistics (N^{obs})	1.0	1.5	2.3	3.2	4.4	6.2	8.6
Background (N^{bgd})	3.3	3.7	4.0	4.2	4.2	4.3	4.4
Acceptance and efficiency	4.5	4.7	4.9	5.2	5.5	6.1	7.1
Total	5.7	6.2	6.7	7.4	8.2	9.7	12.0

atic contributions. The sources of this uncertainty are: (i) the uncertainties on the number of single-muon events in the data and simulation samples, (ii) a 50% uncertainty on the non-W contamination obtained from simulation, (iii) both statistical uncertainties and systematic uncertainties (from PDFs) incorporated to total uncertainty on acceptances and efficiencies. A summary of the contributions of these uncertainties, added in quadrature to get the total error on the W+jets background, is shown in Table 7.

Remaining background contributions come from diboson, QCD multijet, top and $\mathrm{Z} \to \ell^+\ell^-$ +jets events. They are estimated using MC and data driven cross section normalisations.

A $p_{\mathrm{T}}(\mathrm{j}_1)$ dependent scale factor derived from comparisons between simulation and data in the QCD rich region $\Delta\phi(E_{\mathrm{T}}^{\mathrm{miss}}, j_2) < 0.3$ is applied to the QCD cross section. The jet counting threshold is varied between 20 and 80 GeV/c and the monojet event selection applied, except for $\Delta\phi(j_1, j_2) < 2.5$, and $N_{jet} < 3$ as these are the cuts which significantly reduce QCD background. QCD simulation is normalised to data in each $p_{\mathrm{T}}(\mathrm{j}_1)$ bin, and we find a scale factor of 1.53 at $p_{\mathrm{T}}(\mathrm{j}_1) > 250\,\mathrm{GeV}/c$, decreasing to 1.35 at $p_{\mathrm{T}}(\mathrm{j}_1) > 550\,\mathrm{GeV}/c$. Uncertainty on this scale factor, both statistical and from the 50% error assigned to non-QCD backgrounds in the region, is added to the 50% uncertainty on the QCD background.

The NNLO cross section of 234.0 pb [35] is used to normalise $\mathrm{t\bar{t}}$ events. To verify this normalisation in data, a control sample of events with a single electron and a single muon ($\mathrm{e}\mu$ events) is derived from the same dataset as the signal search. The basic monojet selection is applied; Preselection, $E_{\mathrm{T}}^{\mathrm{miss}} > 250$ GeV and $\Delta\phi(j_1, j_2) < 2.5$. Events are required to have one well identified particle flow electron, and a particle flow muon of opposite sign. To reject Z+jets events, a cut is placed on the invariant mass of the $\mathrm{e}\mu$ system ($M(e\mu)$): $M(e\mu) > 60$ GeV/c^2. Agreement between data and simulation in this control sample was found to be within 3%. Single top backgrounds account for $< 1\%$ of total background and are estimated using MC with approximate NNLO [35] cross sections.

The diboson (WW, WZ and ZZ) backgrounds are estimated using MC with NLO cross sections [36], using CTEQ PDFs and requiring the invariant mass of the lepton pair $M(ll) > 12\,\mathrm{GeV}/c^2$. Additional diboson background from W+gamma and Z+gamma events are treated inclusively with W+jets and Z+jets. Simulated W+gamma events are combined with W+jets events, so that W+gamma events are treated as part of the large W+jets background. They are therefore estimated as part of the data driven W+jets background shown in Table 6. In the same way, simulated Z+gamma events have been combined with $\mathrm{Z} \to \ell\ell$+jets and $\mathrm{Z} \to \nu\nu$+jets events. The $\mathrm{Z} \to \nu\nu$+gamma background is estimated within the data driven estimation of the $\mathrm{Z} \to \nu\nu$+jets background, shown in Table 3. The $\mathrm{Z} \to \ell\ell$+gamma background is estimated using MC with the $\mathrm{Z} \to \ell\ell$+jets background, which together account for $< 1\%$ of the total background (here, the $\mathrm{Z} \to \ell\ell$+gamma events have an almost negligible contribution and are included only for completeness). Simulated W+jets and Z+jets events that overlap with W+gamma and Z+gamma simulation have been cut to ensure no double counting between samples; events

Table 8: SM background predictions compared with data after passing the selection requirements for various $p_T(j_1)$ thresholds, corresponding to an integrated luminosity of 19.7 fb^{-1}. The uncertainties include both statistical and systematic terms and are considered to be uncorrelated.

$p_T(j_1)$ (GeV/c)	> 250	> 300	> 350	> 400	> 450	> 500	> 550
$Z \to \nu\nu$+jets	21209±1115	10077±592	4597±324	2250±197	1250±137	663±94	334±65
W+jets	12328±707	5939±366	2690±180	1246±92	627±52	301±29	150±18
$t\bar{t}$	602±301	344±172	178±89	91±46	48±24	27±14	18±9.0
$Z \to \ell\ell$+jets	127±64	75±38	40±20	25±13	17±8.3	11±5.6	7.4±3.7
Single t	172±86	97±49	49±24	21±10	11±5.7	5.2±2.6	3.2±1.6
QCD Multijets	786±473	508±306	304±184	162±99	80±49	52±32	28±18
DiBoson	639±320	369±184	206±103	113±56	64±32	36±18	21±10
Total SM	35862±1474	17409±803	8064±437	3907±250	2098±160	1096±106	563±71
Data	36582	17646	8119	3896	1898	1003	565

from PYTHIA which have a prompt photon with $p_T > 5$ GeV/c, radiated from a quark or antiquark, are removed from W+jets and Z+jets simulation.

A 50% uncertainty is assigned to these background estimations. An additional uncertainty on the QCD background, arising from the scale factor calculation, increases the total QCD uncertainty to approximately 60%.

6 Results

A summary of the predictions and corresponding uncertainties for all the SM backgrounds compared to the data for different values of $p_T(j_1)$ is shown in Table 8. No significant deviation from the SM predictions is observed.

7 Interpretation

To interpret a consistency of the observed number of events with the background expectation in the context of top squarks decaying to a charm and an LSP, limits are set on the production cross section of top squarks as a function of the top squark mass and the LSP mass in the context of $\tilde{t} \to c\tilde{\chi}^0$ decays. Signal acceptance is greatest for large top squark mass and small mass differences, where the final state charm jets are softest and events are most boosted; these events are most 'monojet' like. Signal acceptances at $p_T(j_1) > 300$ GeV/c for all mass points studied are shown in Fig 5.

The selection of signal events (and therefore the signal acceptance) in this analysis relies on a high-p_T ISR jet, so the modelling of ISR must be reliable. The predicted and measured p_T spectra of recoiling systems against ISR jets is studied in [37] for Z+jets, $t\bar{t}$ and other processes and the simulation is found to over predict the data by 20% for ISR jets with $p_T > 250$ GeV/c. All signal acceptances have therefore been weighted to correct for this difference between data and simulation.

The total systematic uncertainty on the signal is found to be 25%. This uncertainty is dominated by the mismodelling of ISR jets, which is assigned an uncertainty of 20% to account for the above-mentioned difference between data and simulation for ISR jets with $p_T > 250$ GeV/c. Also considered are the jet energy scale uncertainty ($< 5\%$ from the change in acceptance when varying energy scales up and down), PDFs ($\approx 5\%$) [34, 38], and the difference in acceptance that is obtained from generating signal events with up to 3 partons in MADGRAPH rather than

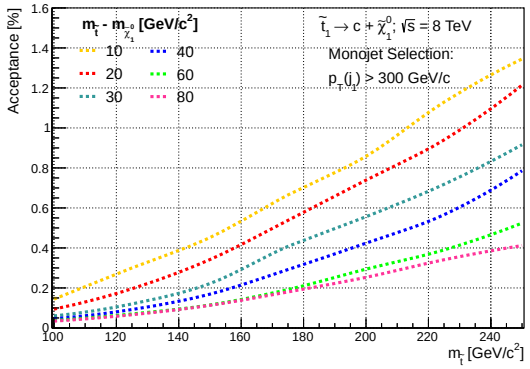

Figure 5: Signal acceptances at $p_{\mathrm{T}}(\mathrm{j}_1) > 300$ GeV/c for all mass points studied. The acceptance is greatest for small mass differences and large top squark mass where the signal is most 'monojet' like. Acceptance values shown are before reweighting due to ISR mis-modelling.

2 partons ($< 4\%$ for $p_{\mathrm{T}}(\mathrm{j}_1) > 500$ GeV/c). The error on the luminosity measurement is 2.6% [39].

The CL_s method is used to estimate a 95% credible interval limit for a signal cross section in a counting experiment [40]. Given the integrated luminosity, signal acceptance, background expectation and number of observed events (with associated uncertainties), the 95% CL upper limit on the signal cross section is set. Expected limits are calculated as a function of $p_{\mathrm{T}}(\mathrm{j}_1)$ for every $(m_{\tilde{\mathrm{t}}}, m_{\tilde{\chi}^0})$ using the background expectation in each signal region. The signal region where the best (ie. lowest) expected limit is found is selected as the optimal region in which to set limits for that mass point. Figure 6 shows the optimised expected and observed limits on the production cross section as a function of the top squark mass for mass differences between the top squark and LSP $(m_{\tilde{\mathrm{t}}} - m_{\tilde{\chi}^0})$ of $10, 20, 30, 40, 60$ and 80 GeV/c^2. Figure 7 shows 95% CL expected $\pm 1\sigma_{\mathrm{exp}}$ and observed limits $\pm 1\sigma_{\mathrm{theory}}$ on the top squark production cross section as a function of top squark mass and LSP mass, and top squark mass and ΔM. Signal cross sections include resummation of soft gluon emission at next-to-leading-logarithmic accuracy (NLO+NLL) [41–45]. Theory uncertainties are dominated by PDF uncertainties and calculations are detailed in [46].

The softer the charm jets in the final state, the more 'monojet'-like an event appears. To be within the signal acceptance, an invisible final state is required; final state charm jets must fall below the jet counting threshold at 60 GeV/c. Charm jets are increasingly soft as mass splittings decrease below 10 GeV/c^2, therefore signal acceptance increases. For this reason, mass splittings smaller than 10 GeV/c^2 are also excluded; the acceptance increases as ΔM decreases, leading to a stronger limit.

Limits are therefore set in an area of phase space unavailable to previous searches, down to small mass splittings. We exclude the region above a line which goes approximately from $(m_{\tilde{\mathrm{t}}} = 120$ GeV/c^2 , $m_{\tilde{\chi}^0} = 50$ GeV/$c^2)$ to $(m_{\tilde{\mathrm{t}}} = 250$ GeV/c^2 , $m_{\tilde{\chi}^0} = 240$ GeV/$c^2)$. As the charm jets in this interpretation are invisible, the limits set can be generalised to $\tilde{\mathrm{t}} \to x\tilde{\chi}^0$ where x is any state invisible to our analysis cuts.

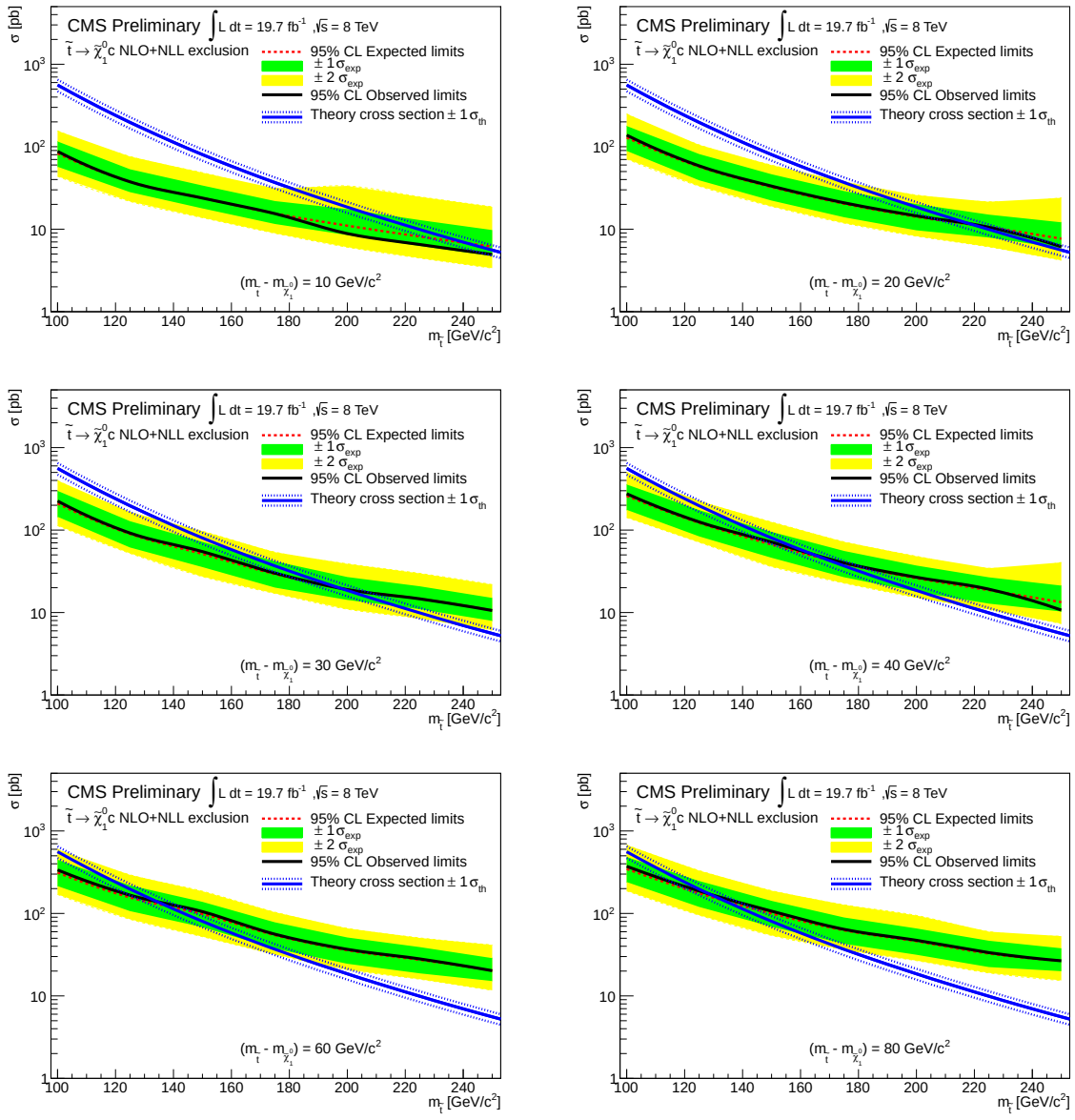

Figure 6: Observed and expected limits on top squark production cross section as a function of the top squark mass for $\Delta M = 10, 20, 30, 40, 60$ and $80\,\mathrm{GeV}/c^2$.

8 Conclusions

A search has been performed for signatures of top squark production in the monojet and $E_{\mathrm{T}}^{\mathrm{miss}}$ channel using 19.7 fb^{-1} of pp collisions at $\sqrt{s} = 8$ TeV. Contributions from $\mathrm{t\bar{t}}$ and QCD multijet processes are reduced to a small level using topological selections. The dominant backgrounds after the complete selection has been applied are from $\mathrm{Z} \to \nu\bar{\nu}$ and W+jet events. These are estimated from data samples of $\mathrm{Z} \to \mu\mu$ and $\mathrm{W} \to \mu\nu$ events. The data are found to be in good agreement with expected contributions from SM processes. Limits on the top squark production cross section are set in a mass parameter space insensitive to previous searches, where mass splittings between $\tilde{\mathrm{t}}$ and $\tilde{\chi}^0$ are 80 GeV/c^2 to less than 10 GeV/c^2. A top squark mass less than 250 GeV/c is also excluded if $\Delta M < 10$ GeV/c.

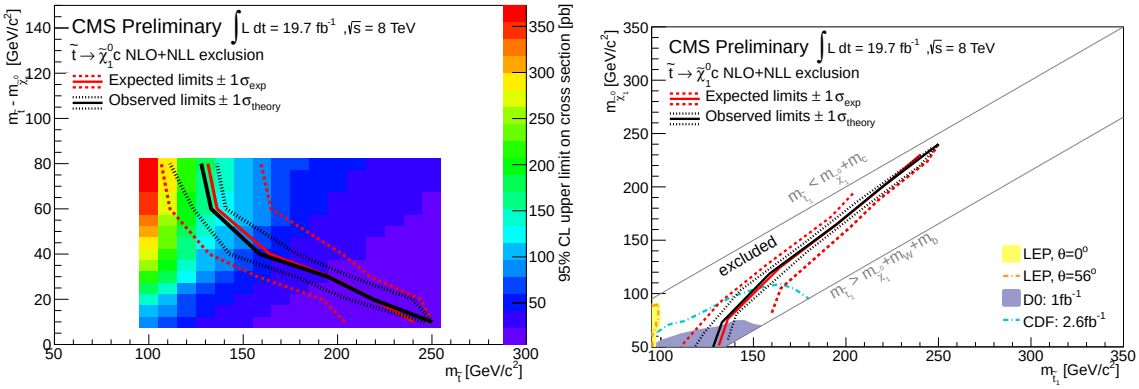

Figure 7: Observed and expected $\pm 1\sigma$ limits on top squark production cross section on both the ($m_{\tilde{t}}$, $m_{\tilde{\chi}^0}$) and ($m_{\tilde{t}}$, $m_{\tilde{t}} - m_{\tilde{\chi}^0}$) mass planes. The colour plot shows the observed production cross section for each mass point.

References

[1] J. Wess and B. Zumino, "Supergauge transformations in four dimensions", *Nuclear Physics B* **70** (1974), no. 1, 39 – 50, doi:http://dx.doi.org/10.1016/0550-3213(74)90355-1.

[2] S. Dimopoulos and H. Georgi, "Softly broken supersymmetry and SU(5)", *Nuclear Physics B* **193** (1981), no. 1, 150 – 162, doi:http://dx.doi.org/10.1016/0550-3213(81)90522-8.

[3] H. Nilles, "Supersymmetry, supergravity and particle physics", *Physics Reports* **110** (1984), no. 12, 1 – 162, doi:http://dx.doi.org/10.1016/0370-1573(84)90008-5.

[4] H. Haber and G. Kane, "The search for supersymmetry: Probing physics beyond the standard model", *Physics Reports* **117** (1985), no. 24, 75 – 263, doi:http://dx.doi.org/10.1016/0370-1573(85)90051-1.

[5] R. Barbieri, S. Ferrara, and C. Savoy, "Gauge models with spontaneously broken local supersymmetry", *Physics Letters B* **119** (1982), no. 46, 343 – 347, doi:http://dx.doi.org/10.1016/0370-2693(82)90685-2.

[6] S. Dawson, E. Eichten, and C. Quigg, "Search for supersymmetric particles in hadron-hadron collisions", *Phys. Rev. D* **31** (Apr, 1985) 1581–1637, doi:10.1103/PhysRevD.31.1581.

[7] S. P. Martin, "A Supersymmetry primer", arXiv:hep-ph/9709356.

[8] D. Chung et al., "The Soft supersymmetry breaking Lagrangian: Theory and applications", *Phys.Rept.* **407** (2005) 1–203, doi:10.1016/j.physrep.2004.08.032, arXiv:hep-ph/0312378.

[9] S. P. Martin, "Compressed supersymmetry and natural neutralino dark matter from top squark-mediated annihilation to top quarks", *Phys.Rev.* **D75** (2007) 115005, doi:10.1103/PhysRevD.75.115005, arXiv:hep-ph/0703097.

[10] S. P. Martin, "The Top squark-mediated annihilation scenario and direct detection of dark matter in compressed supersymmetry", *Phys.Rev.* **D76** (2007) 095005, doi:10.1103/PhysRevD.76.095005, arXiv:0707.2812.

[11] M. Carena, A. Freitas, and C. Wagner, "Light Stop Searches at the LHC in Events with One Hard Photon or Jet and Missing Energy", *JHEP* **10** (2008) 109, doi:10.1088/1126-6708/2008/10/109, arXiv:0808.2298.

[12] C. Balazs, M. S. Carena, and C. Wagner, "Dark matter, light stops and electroweak baryogenesis", *Phys.Rev.* **D70** (2004) 015007, doi:10.1103/PhysRevD.70.015007, arXiv:hep-ph/0403224.

[13] K.-i. Hikasa and M. Kobayashi, "Light scalar top quark at e^+e^- colliders", *Phys. Rev. D* **36** (Aug, 1987) 724–732, doi:10.1103/PhysRevD.36.724.

[14] C. Boehm, A. Djouadi, and Y. Mambrini, "Decays of the lightest top squark", *Phys. Rev. D* **61** (Apr, 2000) 095006, doi:10.1103/PhysRevD.61.095006.

[15] CMS Collaboration, "Search for new physics in monojet events in pp collisions at $\sqrt{s}$= 8 TeV", CMS Physics Analysis Summary CMS-PAS-EXO-12-048, (2013).

[16] CMS Collaboration, "The CMS experiment at the CERN LHC", *JINST* **3** (2008) S08004, doi:10.1088/1748-0221/3/08/S08004.

[17] CMS Collaboration, "Particle–Flow Event Reconstruction in CMS and Performance for Jets, Taus, and $E_{\mathrm{T}}^{\mathrm{miss}}$", CMS Physics Analysis Summary CMS-PAS-PFT-09-001, (2009).

[18] M. Cacciari, G. P. Salam, and G. Soyez, "The anti-k_t jet clustering algorithm", *JHEP* **04** (2008) 063, doi:10.1088/1126-6708/2008/04/063, arXiv:0802.1189.

[19] CMS Collaboration, "Determination of jet energy calibration and transverse momentum resolution in CMS", *JINST* **6** (2011) P11002, doi:10.1088/1748-0221/6/11/P11002, arXiv:1107.4277.

[20] CMS Collaboration, "Performance of muon identification in pp collisions at $\sqrt{s}$ = 7 TeV", CMS Physics Analysis Summary CMS-PAS-MUO-10-002, (2010).

[21] CMS Collaboration, "Performance of τ-lepton reconstruction and identification in CMS", *JINST* **7** (2012) 1001, doi:10.1088/1748-0221/7/01/P01001, arXiv:1109.6034.

[22] J. Alwall et al., "MadGraph/MadEvent v4: the new web generation", *JHEP* **09** (2007) 028, doi:10.1088/1126-6708/2007/09/028, arXiv:0706.2334.

[23] T. Sjöstrand, S. Mrenna, and P. Z. Skands, "PYTHIA 6.4 physics and manual", *JHEP* **05** (2006) 026, doi:10.1088/1126-6708/2006/05/026, arXiv:hep-ph/0603175.

[24] R. Field, "Early LHC Underlying Event Data - Findings and Surprises", arXiv:1010.3558.

[25] J. Pumplin et al., "New generation of parton distributions with uncertainties from global QCD analysis", *JHEP* **07** (2002) 012, doi:10.1088/1126-6708/2002/07/012, arXiv:hep-ph/0201195.

[26] CMS Collaboration Collaboration, "Interpretation of Searches for Supersymmetry with simplified Models", arXiv:1301.2175.

[27] M. L. Mangano, M. Moretti, and R. Pittau, "Multijet matrix elements and shower evolution in hadronic collisions: W $b\bar{b}$ + n jets as a case study", *Nucl. Phys. B* **632** (2002) 343, doi:10.1016/S0550-3213(02)00249-3, arXiv:hep-ph/0108069.

[28] GEANT4 Collaboration, "GEANT 4 – a simulation toolkit", *Nucl. Inst. Meth.* **506** (2003) 250, doi:10.1016/S0168-9002(03)01368-8.

[29] CMS Collaboration, "CMS tracking performance results from early LHC operation", *Eur. Phys. J. C* **70** (2010) 1165, doi:10.1140/epjc/s10052-010-1491-3, arXiv:1007.1988.

[30] Particle Data Group Collaboration, "Review of Particle Physics", *J. Phys. G* **37** (2010) 075021, doi:10.1088/0954-3899/37/7A/075021.

[31] A. Martin, W. Stirling, R. Thorne, and G. Watt, "Parton distributions for the LHC", *Eur.Phys.J.* **C63** (2009) 189–285, doi:10.1140/epjc/s10052-009-1072-5, arXiv:0901.0002.

[32] R. D. Ball et al., "Impact of Heavy Quark Masses on Parton Distributions and LHC Phenomenology", *Nucl.Phys.* **B849** (2011) 296–363, doi:10.1016/j.nuclphysb.2011.03.021, arXiv:1101.1300.

[33] J. Pumplin et al., "New generation of parton distributions with uncertainties from global QCD analysis", *JHEP* **0207** (2002) 012, doi:10.1088/1126-6708/2002/07/012, arXiv:hep-ph/0201195.

[34] M. Botje et al., "The PDF4LHC Working Group Interim Recommendations", (2011). arXiv:1101.0538.

[35] N. Kidonakis, "Differential and total cross sections for top pair and single top production", doi:10.3204/DESY-PROC-2012-02/251, arXiv:1205.3453.

[36] J. M. Campbell, R. K. Ellis, and C. Williams, "Vector boson pair production at the LHC", *JHEP* **1107** (2011) 018, doi:10.1007/JHEP07(2011)018, arXiv:1105.0020.

[37] CMS Collaboration, "Search for top-squark pair production in the single-lepton final state in pp collisions at $\sqrt{s} = 8$ TeV", arXiv:1308.1586.

[38] M. Krämer et al., "Supersymmetry production cross sections in pp collisions at $\sqrt{s} = 7$ TeV", arXiv:1206.2892.

[39] CMS Collaboration, "CMS Luminosity Based on Pixel Cluster Counting - Summer 2013 Update", CMS Physics Analysis Summary CMS-PAS-LUM-13-001, (2013).

[40] L. Moneta, K. Cranmer, G. Schott, and W. Verkerke, "The RooStats Project", in *Proceedings of the 13th International Workshop on Advanced Computing and Analysis Techniques in Physics Research (ACAT2010)*. SISSA, 2010. arXiv:1009.1003.

[41] W. Beenakker, R. Hopker, M. Spira, and P. Zerwas, "Squark and gluino production at hadron colliders", *Nucl.Phys.* **B492** (1997) 51–103, doi:10.1016/S0550-3213(97)80027-2, arXiv:hep-ph/9610490.

[42] A. Kulesza and L. Motyka, "Threshold resummation for squark-antisquark and gluino-pair production at the LHC", *Phys.Rev.Lett.* **102** (2009) 111802, doi:10.1103/PhysRevLett.102.111802, arXiv:0807.2405.

[43] A. Kulesza and L. Motyka, "Soft gluon resummation for the production of gluino-gluino and squark-antisquark pairs at the LHC", *Phys.Rev.* **D80** (2009) 095004, doi:10.1103/PhysRevD.80.095004, arXiv:0905.4749.

[44] W. Beenakker et al., "Soft-gluon resummation for squark and gluino hadroproduction", *JHEP* **0912** (2009) 041, doi:10.1088/1126-6708/2009/12/041, arXiv:0909.4418.

[45] W. Beenakker et al., "Squark and Gluino Hadroproduction", *Int.J.Mod.Phys.* **A26** (2011) 2637–2664, doi:10.1142/S0217751X11053560, arXiv:1105.1110.

[46] M. Krämer et al., "Supersymmetry production cross sections in pp collisions at $\sqrt{s} = 7$ TeV", arXiv:1206.2892.